The AAPS Journal (2019) 21: 94
DOI: 10.1208/s12248-019-0361-7

Research Article

Evaluating a Multiscale Mechanistic Model of the Immune System to Predict Human Immunogenicity for a Biotherapeutic in Phase 1

Lora Hamuro,[1] Giridhar S. Tirucherai,[1] Sean M. Crawford,[2] Akbar Nayeem,[3] Renuka C. Pillutla,[2] Binodh S. DeSilva,[4] Tarek A. Leil,[5] and Craig J. Thalhauser[5,6]

Received 18 December 2018; accepted 28 June 2019; published online 24 July 2019

Abstract. A mechanistic model of the immune response was evaluated for its ability to predict anti-drug antibody (ADA) and their impact on pharmacokinetics (PK) and pharmacodynamics (PD) for a biotherapeutic in a phase 1 clinical trial. Observed ADA incidence ranged from 33 to 67% after single doses and 27–50% after multiple doses. The model captured the single dose incidence well; however, there was overprediction after multiple dosing. The model was updated to include a T-regulatory (Treg) cell mediated tolerance, which reduced the overprediction (relative decrease in predicted incidence rate of 21.5–59.3% across multidose panels) without compromising the single dose predictions (relative decrease in predicted incidence rate of 0.6–13%). The Treg-adjusted model predicted no ADA impact on PK or PD, consistent with the observed data. A prospective phase 2 trial was simulated, including co-medication effects in the form of corticosteroid-induced immunosuppression. Predicted ADA incidences were 0–10%, depending on co-medication dosage. This work demonstrates the utility in applying an integrated, iterative modeling approach to predict ADA during different stages of clinical development.

KEY WORDS: Pharmacokinetics; Anti-drug antibodies; Immunogenicity; Mechanistic model.

INTRODUCTION

Biotherapeutic proteins can induce a humoral immune response that may lead to anti-drug antibody (ADA) production. ADAs have potential to impact pharmacokinetics (PK), pharmacodynamics (PD), and downstream safety and efficacy, requiring ADA formation to be closely monitored throughout clinical development (1). Biotherapeutics are designed, manufactured, and formulated to minimize immunogenicity, but most biotherapeutics still have some level of detectable ADA when tested in humans that may or may not be clinically relevant (2).

Historically, it has been shown that ADA formation can depend on many factors that are generally categorized into drug-specific (*i.e.*, amino acid sequence, glycosylation, protein folding), production-specific (*i.e.*, impurities, aggregates, leachates), and patient-specific (*i.e.*, HLA type, age, co-medications, disease state) (1). Our understanding of how these risk factors contribute to ADA formation in humans is continuing to evolve, but the underlying biology of the adaptive immune response to an antigenic peptide sequence that can result in antibody formation has been well characterized (3). Mechanistic models are especially well-suited to integrate this knowledge to generate predictions in novel contexts.

In 2014, Chen *et al.* published a multiscale mechanistic model of the adaptive immune response to predict ADA formation for biotherapeutic proteins, and applied the model to retrospectively predict the immunogenicity for adalimumab (4,5). The Chen *et al.* model will be referred to as the CHV (Chen, Hickling, Vicini) model and is unique with respect to past models of immunogenicity in that it links protein sequence–based T cell epitope prediction methods to downstream processes central to the immune response: antigen presentation and the T and B cell biology required for ADA production (Table I). When combined with a drug disposition model, it can also be used to predict the impact on the PK and PD of the drug. Since this model can reproduce important aspects of the immune system such as (1) affinity maturation and IgM to IgG class switching, (2) development

Electronic supplementary material The online version of this article (https://doi.org/10.1208/s12248-019-0361-7) contains supplementary material, which is available to authorized users.

[1] Clinical Pharmacology and Pharmacometrics, Bristol-Myers Squibb, Princeton, New Jersey 08543, USA.
[2] Bioanalytical Sciences, Translational Medicine, Bristol-Myers Squibb, Princeton, New Jersey 08543, USA.
[3] Molecular Structure and Design, Bristol-Myers Squibb, Princeton, New Jersey 08543, USA.
[4] Analytical Strategy and Operations, Product Development, Bristol-Myers Squibb, Princeton, New Jersey 08543, USA.
[5] Quantitative Clinical Pharmacology, Bristol-Myers Squibb, Route 206 & Province Line Road, Princeton, New Jersey 08543, USA.
[6] To whom correspondence should be addressed. (e–mail: craig.thalhauser@bms.com)

Table I. System Levels Included in the Multiscale Immunogenicity Model by Chen *et al.*[5]

System level	Biology described
Subcellular	Intracellular protein processing and MHCII peptide loading
Cellular*	DC antigen presentation, T cell and B cell activation and differentiation
Tissue/plasma	ADA production, drug, and drug target disposition
Patient level	MHCII haplotype

*A T regulatory cell feedback mechanism was added to the previously published model to reduce overprediction bias and improve model predictability

of a memory response, and (3) anticipated time-scale for T and B cell activation and proliferation (5), we wanted to evaluate the ability of the model to predict ADA formation for a novel biotherapeutic and compare our predictions with the ADA data collected in the phase 1 clinical trial.

Here we report the use of the CHV model (4,5) to predict ADA incidence for different doses, regimens, and corticosteroid use and to evaluate the impact of these variables on the PK and PD for ATI-1465 a biotherapeutic, Fc-fusion protein in early clinical development (6).

METHODS

Clinical Study

The safety, tolerability, and PK for ATI-1465 was evaluated after subcutaneous administration of a combined single ascending dose (SAD) and multiple ascending dose (MAD) study in healthy volunteers conducting in the US in accordance with ethical standards for trial conduct and monitoring. The trial was a randomized, placebo-control, double-blind combined SAD and MAD trial with five single dose levels (5, 15, 45, 90, and 180 mg) in the SAD portion and four multi dose levels of ATI-1465 administered SC once weekly dosing (Q1W) (days 1, 8, 15, 22, and 29; at 15, 45, 90, or 180 mg). In a fifth panel, three 45 mg doses of ATI-1465 was administered SC every 2 weeks (Q2W) (days 1, 15, and 29).

Bioanalytical Methodology for ADA Detection

A validated bioanalytical method was used to detect anti-drug antibodies in human serum samples. The method was comprised of three tiers: (1) a screening assay, which identified putative positive samples using a 95% cutpoint; (2) a confirmatory assay (99% cutpoint), which confirmed specificity of the screened positive samples after adding excess drug; and (3) a titer assay, which determined the magnitude of the positive response (see Supplemental on assays for validated assay specifications). The assay sensitivity was 10 ng/ml with a drug tolerance of 50 μg/mL. The maximum drug concentration observed in the clinical trial was 16 μg/mL and within the assay drug tolerance. The method was a direct binding, chemiluminescent enzyme-linked immunosorbant assay (ELISA) that used ATI-1465 as the capture reagent and a detection mixture of goat-HRP-conjugated anti-rabbit Fc (Jackson Immunoresearch, cat# 111-035-144), anti-human kappa/lambda light chain (Southern Biotech cat# 2070-05, cat# 2060-05) as the detection reagent. Drug-affinity purified rabbit polyclonal anti-drug IgG was the positive control. To convert titer results into mass units for comparison with the model predictions, the positive control was used as a standard curve to calculate a relative concentration in ng/mL for each sample using the instrument response values. Predicting molar amounts of human ADA is an approximation, since human ADA can potentially bind with different affinities and avidities relative to the animal positive control.

Antigenic Peptide Predictions

The ATI-1465 protein sequence was screened using a publically available Immune Epitope Data Base (IEDB) (Immune Epitope Database) (http://www.iedb.org) (7). A 15-mer peptide walk-through of the entire sequence using a 1-residue right shift starting from the N-terminus was used to search for peptide regions with high predicted binding affinity to 41 different MHCII (HLA-DRB) (human leukocyte antigen) alleles. The HLA system is a gene complex encoding the major histocompatibility complex (MHC) proteins class I and II of which the MHC II display endocytosed, antigenic peptides to CD4+ T cells. Three classical MHC Class II heterodimeric receptors (HLA-DR, HLA-DP, and HLA-DQ) are included in the CHV model. HLA-DR (specifically HLA-DRB) contains the most genetic diversity and was the focus of the in silico screening. In total 111, 15-mers were screened and one region in the active binding loop of ATI-1465 was predicted to be antigenic based on strong binding (IC50 ≤ 200 nM) of several overlapping peptides in this region to several of the tested MHCII (HLA-DRB1) alleles (Table II) (8). These peptide sequences were predicted to not exist in the human proteome using blastp, the National Center for Biotechnology Information (NCBI) sponsored database (9).

Table II. Predicted IC50s for a Peptide in the Active Loop of ATI-1465 for 8 Representative HLA-DRB Alleles

MHCII-HLA-DRB allele	Allele frequency American population (%)	IEDB IC50 prediction (nM)
DRB1*0101	6.6	16
DRB1*0301	10	884
DRB1*0401	6	125
DRB1*0701	11.5	40
DRB1*0901	1.5	110
DRB1*1101	5.5	44
DRB1*1301	5.0	355
DRB1*1501	10.4	71

IEDB Immune Epitope Data Base (IEDB) (http://www.iedb.org)

Data Analysis Platform

The mathematical equations describing the immune system CHV model (5) were used to establish the model in Matlab® R2015a and R2016a software (Mathworks®). All model optimizations, diagnostic graphics, simulations, and post-processing were conducted in Matlab®.

Model Development

The model included a predicted antigenic sequence that was identified in the in silico MHC-II binding screen to have the highest binding to the **8** most frequent DRB (HLA-DB) alleles out of 41 DRB alleles in the American population compared to other antigenic sequences (Table II). The peptide mapped to the non-Fc, variable loop region of ATI-1465. Binding affinities to 41 representative HLA-DRB alleles in the American population were obtained from the NetMHCIIpan module in IEDB. Binding affinities to HLA-DP and HLA-DQ were assigned values of 4 μM (several orders of magnitude higher IC50) as in the CHV model (5). A PKPD drug disposition model specific to the compound was included along with the parameter estimates from a previously established population model and ADA incorporated as a competitive inhibitor of target binding (Fig. 1) (10). The equations and the parameter estimates can be found in the Supplemental.

The CHV model was modified to include T-regulatory (Tregs) cells to evaluate the potential to reduce the ADA overprediction bias. The Tregs were incorporated in the model according to the previously described cross regulation model (11,12) . Briefly, Tregs interfere with the ability of activated effector T cells to proliferate (activated T cells designated as $AT_{N\ (naive)}$, $AT_{M\ (mature)}$ in the CHV model). Tregs themselves are induced by activated effector cells in the presence of an APC displaying a cognate antigen. To match the formulation of the CHV model, we assume that very low levels of activated T cells suppress Treg activation, so that any immune response is not immediately 'swamped' by immunosuppression. The initial number of therapeutic protein sensitive Tregs was obtained from the literature (13–15). A more formal mathematical description of these changes is given below.

Model Modifications

There were three modifications to the CHV model: (1) addition of Treg biology to account for model overprediction after multidose, (2) addition of a drug-specific PKPD disposition model, and (3) modifications to the equations describing the ADA effects on drug and B cells to include the newly defined drug disposition model. The Treg model is described below and the other model changes, including parameters and equations are provided in the supplemental material. All other equations used were not changed from the original publication of the CHV model. Treg cells were added in to the CHV model (4,5) based on the work of Velez de Mendizabal *et al.* (12). The same parameterized forms introduced in the CHV model for T effector cell homeostasis, activation, and proliferation were used, assuming a Treg behaves like a naïve cell for the purposes of activation signal strength requirements. However, since Tregs use the IL-2

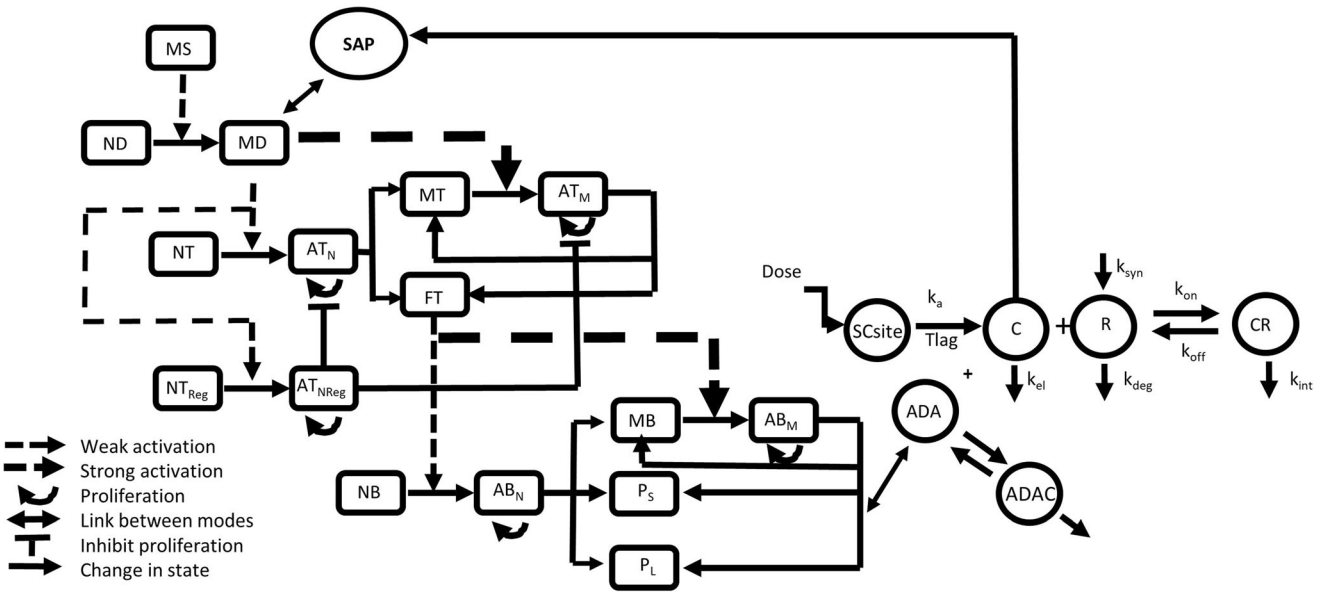

Fig. 1. Schematic overview of the immune system model that includes a PKPD disposition model. Model details of the antigen presentation, T cell biology and B cell biology are presented as in the CHV model (5) with additional model details for T regulatory cell biology. A target mediated PKPD model was used to characterize the drug and target disposition. The drug is absorbed from the SC injection site into the central compartment (C), where it can bind to the target (R) to the form a drug-target complex (RC). In this model ADA is modeled as a direct competitor of target binding. The various rate constants are defined (Tlag = absorption lag, ka = absorption rate constant, kel = drug elimination rate constant, ksyn = target synthesis rate, kdeg = target degradation rate, kon = target binding rate constant, koff = target dissociation rate constant, kint = drug-target complex internalization rate constant. SAP: subcellular antigen processing, MS: maturation signal, ND: naïve Dendritic Cell (DC), MD: mature DC, NT: naïve T cell, ATN: activated naïve T cell, MT: memory T cell, FT: functional T cell, ATM: activated memory T cell, NTReg: naïve Treg cell, ATNReg: activated naïve Treg cell, NB: naïve B cell, ABN: activated naïve B cell, MB: memory B cell, ABM: activated, memory B cell, Ps : plasma cell, short lived, PL: plasma cell, long lived, ADA: anti-Drug antibody, C: drug in central compartment, R: drug target, CR: drug-target complex, ADAC: ADA-drug complex

produced by other activated T cells as their proliferation driver, we modified the E expressions (Eq. 15.1, Supplemental Material, CHV model (4,5) for activated Tregs to be:

$$E_T = \frac{MD}{MD + \sum NT + \sum AT_N + \sum AT_M + \sum MT + \sum Tr + \sum ATr} * \frac{\sum AT_N + \sum AT_M - Ke_{tr}}{\sum AT_N + \sum AT_M + Ke_{tr}}$$

So that in the absence of activated effector T cells, activated Tregs are incapable of proliferating.

Here, E_T is a proliferation/differentiation function describing Tregs. MD = mature dendritic cells, NT = naive T cells, AT_N = activated native T cells, MT = memory T cells, Tr = Tregs, ATr = activated Tregs, AT_M = activated memory T cells, Ke_{tr} = number of effector Tregs required for half-maximal Treg proliferation.

The full differential equations for resting and active Tregs are:

$$\frac{dT_R}{dt} = \beta_{NT} * (Tr0 - Tr) - \delta_{NT} * D_R * Tr + \rho_{AT} * (1 - E_R) * ATr$$

$$\frac{dAT_R}{dt} = \delta_{NT} * D_R * Tr + \rho_{AT} * E_R * ATr - \beta_{AT} * ATr$$

These equations are analogous to Eqs. 14 and 15 from the original CHV model. Where T_R = resting Tregs, AT_R = activated Tregs, β_{NT} = death rate naive T cells, Tr0 = initial number of therapeutic protein sensitive T cells, δ_{NT} = maximum activation rate of naive T cells, D_R = activation function for Tregs, ρ_{AT} = maximum proliferation rate for activated T cells, β_{AT} = death rate of activated T cells. The values for β_{NT}, δ_{NT}, ρ_{AT}, and β_{AT}, and the functional form for D_R, were the same as used in the CHV model. For all T cells, the number of Tregs (active and resting) are included in the D functions (Eq. 14.1 CHV model), to account for increased competition for MHCII on the available DCs.

To account for Treg activity beyond competition effects, we implemented a decreased proliferation rate of activated cells, using the model of Velez de Mendizabal *et al.* as a basis (12). Specifically, we defined:

$$I_{Tr} = \frac{Ki_{Tr}^h}{Ki_{Tr}^h + (\sum ATr)^h}$$

where I_{Tr} is the inhibition effect induced by Tregs, Ki_{Tr}^h = Treg inhibition rate constant, h = slope coefficient for Treg effects, ATr = activated Tregs. T effector cell equations were updated to be:

$$\frac{dAT_X}{dt} = \delta_{XT} * D_{NX} * XT + \rho_{AT} * E_X * AT_X * \mathbf{I_{Tr}} - \beta_{AT} * AT_X$$

Parameter	Definition	Value	Source
Ki_{Tr}	Number of Tregs required for half-maximal suppression	200	Velez de Mendizabal *et al.* (12)
Ke_{Tr}	Number of Teffs required for half-maximal Treg proliferation	1000	Velez de Mendizabal *et al.* (12)
h	Slope coefficient for Treg effects	5	Velez de Mendizabal *et al.* (12)
Tr0	Initial number of therapeutic protein-sensitive Tregs	0.1–10% of NT0	Wilson *et al.* (15), Maddur *et al.* (13), Mukhopadhyay *et al.* (14)

where $X \in \{N, M\}$. The new Treg associated parameters were taken exactly as specified in Velez de Mendizabal *et al.* All the other parameters are exactly as described above in the Treg dynamics, with values identical to those in the CHV publication.

To predict the effects of ADA formation against this region of ATI-1465, the structural population PK model estimated from the phase 1 trial data was included in the model. Keeping in line with the original analysis of adalimumab performed by Chen *et al.*, only variability on clearance (in the form of a log-normal distribution of parameter values with mean and variance as estimated from the data) was used to induce PK variability in our simulations. The structural model also included a state equation for the drug target, including variability in baseline levels and estimates of in vivo binding affinity. These equations allowed us to more fully explore possible consequences of ADA formation on the proximal PD of the compound, by comparing the concentration of free target in the presence and absence of neutralizing ADAs.

Since ATI-1465 is being developed to treat patients who typically also receive daily corticosteroid therapy, the immunosuppressive effects of corticosteroids on lymphocyte proliferation were incorporated in the model. The oral dose of prednisolone used in the simulations was 20 mg and approximates the daily dose that would be given for this indication with a 27 kg body weight (pediatric population) (*i.e.*, 0.75 mg/kg/day). An IC50 of 51.4 nM for prednisolone inhibition of human whole blood lymphocyte proliferation was used (16). The average daily free plasma prednisolone concentration at steady state was estimated to be 30–40 nM in adults (17,18). Since the free plasma concentration is slightly under the IC50, where 50% inhibition is assumed, we thus implemented corticosteroid effects as a decrease in activated lymphocyte proliferation rate simulated at two levels of suppression (25% and 50%) as reasonable expectations for the corticosteroid doses observed in the study.

Model Evaluation

A collection of 30,000 virtual patients was generated by sampling the following parameters from their pre-specified population distributions: (1) MHC-II (HLA-DRB) alleles and their IC50s for the antigenic peptide,

(2) drug clearance, (3) target levels, and (4) number of Tregs required for half-maximal inhibitory effect. For drug clearance and target levels, population mean values and the between-subject variability estimates from the population PK analysis were used to generate distributions. For the MHC-II allele distribution, DRB allele frequencies in the mixed North American population were calculated using data available at dbMHC (https://www.ncbi.nlm.nih.gov/projects/gv/mhc/ihwg.cgi?cmd=PRJOV&ID=9&SHOWMAP=1). Briefly, for populations of African, Asian, and European descent, allele frequencies were averaged across different studies and those frequencies then blended together based on demographic information from the 2010 US Census. Forty-one alleles were ultimately selected, which represented 92% and 100% of the total allelic distribution in the American and Japanese populations, respectively, with all alleles occurring in at least 0.1% of the population. Two alleles were randomly selected for each virtual patient, although virtual patients could have two copies of the same allele. Each virtual patient was simulated with the new Treg module active and inactive, for each dose panel used in the phase 1 trial. Trial simulations were performed by randomly selecting 6 subjects per dose group for the SAD phase of the trial and 12 subjects per dose group for the MAD phase. A total of 500 such trial simulations were conducted for each dose level. For each trial simulation, the number of ADA positive subjects and the magnitude of the response at different times after dosing were summarized. An ADA positive subject in the simulation was defined as a subject that had ADA levels ≥ 10 ng/mL (≥ 0.067 nM) at a time point of interest. This threshold was the assay sensitivity determined using the positive anti-drug antibody control to detect ADA. The 500 simulated trials were summarized using histograms to indicate the predicted number of positive ADA subjects (out of the total number of subjects simulated) for each trial and compared to the observed ADA incidence. The predicted time profiles for ADA production and impact to PK and PD were also plotted (Figs. 4 and 5). ADA binding was modeled as directly binding to the drug and accelerating drug clearance, preventing interaction with the target as illustrated in Fig. 1. Model predictions were compared using the mean predicted ADA+ subjects and standard deviation for the trial simulations.

Data Exclusion

In the SAD portion of the phase 1 study, two subjects were baseline ADA positive prior to the first dose. While the model could in principle be adapted to reproduce such a finding (by setting non-zero initial conditions for certain key players in the immune cascade, most importantly the presence of existing compound-reactive memory B cells and long lived plasma cells), there were insufficient data available to estimate the likelihood of this occurring in the general population with confidence, nor did we have any insight into the presence or absence of reactive T cells to the compound, since the B cells may be targeting a different epitope than the T cells. Thus, we decided to exclude those two subjects from this analysis. To account for these missing patients, simulated trials for the SAD1 and SAD5 dose panels were populated with 5 virtual patients, not 6, and compared to the trial data exclusive of the baseline ADA positive subjects.

RESULTS

Observed ADA in Phase 1

ADA levels were measured in serum at pretreatment and on days 15, 36, 49, 63, 77, and 91 after a single dose and on days 15, 36, 71, 85, 99, and 120 after multiple doses of ATI-1465. At day 91, after single dose, ADA incidence ranged from 33 to 67% across the dose panels with a total ADA incidence of 47% (Table III). ADA was not dependent on dose after single dose with lower doses having similar incidences as higher doses at day 91, suggesting that the antigenic threshold for immune cell activation was reached at the lowest dose. However, there is evidence of a bell-shape response in the MAD panels. ADA incidence was the highest in the lowest dose MAD panel 50% (3/6) that decreased to 25% (3/12) in the highest MAD panel (Table III). Although the numbers are small, this may support tolerance being developed at higher doses. ADA titers were low and ranged from 2 to 64 and were not a consequence of the inability to detect ADA, since the drug tolerance of the assay was higher than the observed drug levels. Two subjects in the SAD panels had pretreatment confirmed baseline positive ADA (titer = 4), whose titers increased post treatment, suggesting a pre-existing response that may have been boosted post treatment. The majority of the ADA positive subjects (10/14 = 71%) seroconverted between day 49 and day 91. At day 120 after multiple weekly (or every other week) doses, the incidence ranged from 25 to 50%. Titers were again low (< 16) with the majority of ADA positive subjects (14/17 = 82%) seroconverting at or after day 71. Given the observed ADA incidence, it was important to reevaluate the amino acid sequence to identify any predicted antigenic T cell epitopes.

Table III. Observed ADA at Day 91 for Each Dose Level After Single Dose and at Day 120 After 5 Weekly Multiple Doses (Q4W)

Panel (dose)	Total subjects	Observed no. of ADA positive subjects (%)
SAD 1 (5 mg)	6	3 (50)
SAD 2 (15 mg)	6	2 (33)
SAD 3 (45 mg)	6	4 (67)
SAD 4 (90 mg)	6	2 (33)
SAD 5 (180 mg)	6	3 (50)
SAD total	30	14 (47)
MAD 1 (15 mg) QW	6	3 (50)
MAD 2 (45 mg) QW	12	4 (33)
MAD 3 (90 mg) QW	12	4 (33)
MAD 4 (180 mg) QW	12	3 (25)
MAD 5 (45 mg) Q2W	11	3 (27)
MAD total	53	17 (32)

Predicted Antigenic Peptide Sequence

A prerequisite for the immunogenicity model was the ability to predict an antigenic sequence that provided the initiation trigger for antigen presentation by dendritic cells. Since most available MHCII binding prediction tools consider peptides of 15 residues in length, all sequential peptides of this length generated from the sequence of ATI-1465 were scanned against both the binding prediction algorithm NetMHCIIpan v3.0 (19) and the human proteome to detect germline sequences (9). A single peptide in the active loop region of ATI-1465 was predicted to bind with high affinity (IC50 < 200 nM) to several of the 41 MHCII DRB alleles for which population distribution data was gathered and showed significant non-homology to the human proteome, and so was used as the antigenic input to the model. Since these 41 alleles do not quite cover the entirety of the target population (total representation was ~ 93%), a 42nd allele termed "other" was included with its affinity for the antigenic compound set at 4 μM.

ADA Predictions Using Previously Published Model

The distributions of 42 DRB alleles in three different world populations (US, Japanese, and European) were calculated using the data available at dbMHC (20). Accounting for this variability as well as the variability established in clearance and initial target load, the CHV model was used to simulate 500 replicate SAD trials of 6 patients each for each dose panel assessed in the trial. After each simulated trial, the number of virtual patients showing ADA > 10 ng/ml was recorded, and the results are shown in Fig. 2 (orange histogram). In general, the model shows an increase in ADA incidence as the antigen exposure increases; this is primarily due to increasing numbers of MHCII DRB alleles in the population that have met the EC50 binding threshold as the doses increase and are now capable of binding and displaying sufficient antigen to induce a T cell response.

Next, the simulation procedure was repeated to simulate multiple dosing of 4 weekly doses (QW) at 5 different dose levels (5 MAD dose panels) (Fig. 3 (orange histograms)). We note now, contrary to our findings in the SAD simulation, the model is significantly overpredicting ADA incidence; indeed, overall incidence was reduced in the MAD panel relative the SAD. We hypothesized that inclusion of a Treg-based tolerance mechanism into the model, based on previously described models with no extra parameter estimation required, would be sufficient to describe this trend of decreased ADA incidence.

ADA Predictions Incorporating T Regulatory Cell Tolerance

Tregs were added to the model such that their effects were to decrease antigen-dependent T cell proliferation. Using this framework, we re-simulated 500 replicates of both the SAD and MAD trials. These results are shown in Fig. 2 and Fig. 3 (blue histograms). We note firstly that inclusion of the Treg tolerance mechanism led to only minor changes in

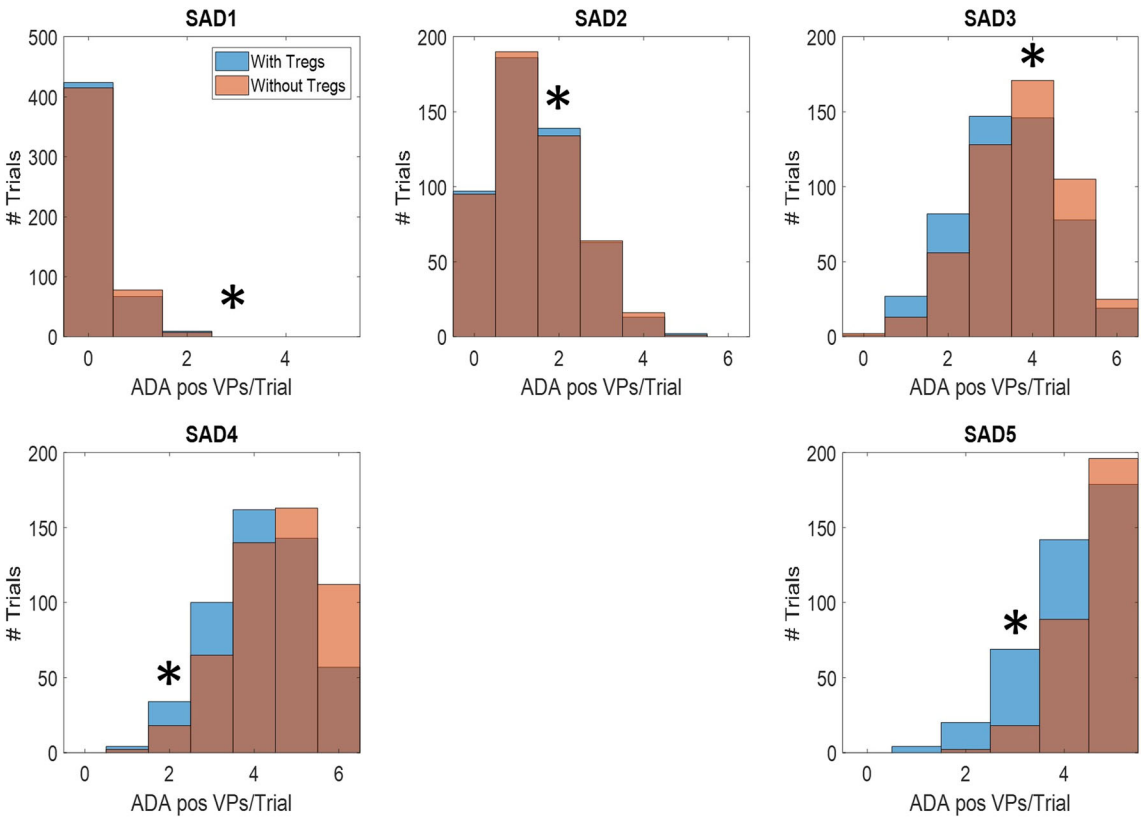

Fig. 2. Trial simulation histograms of ADA incidence for the virtual patient (VP) population at all 5 dose levels at day 91 after subjects received a single dose. The observed number of ADA positive (ADA pos) subjects for that dose panel is indicated with an asterisk. Histograms from the original model are orange (without Tregs), overlaid with histograms from the Treg adjusted model in blue (with Tregs)

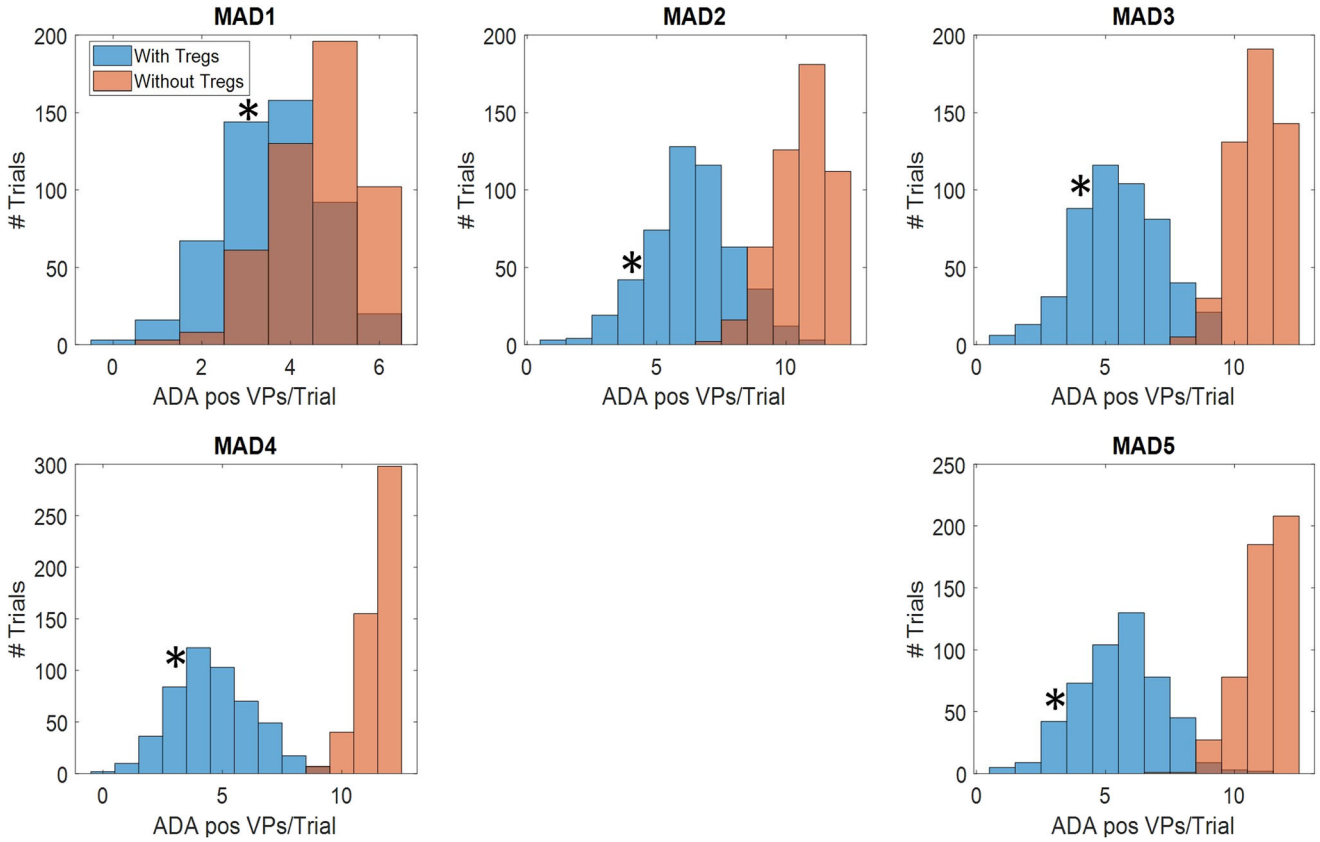

Fig. 3. Trial simulation histograms of ADA incidence for the virtual patient (VP) population at all 5 dose levels at day 120 after subjects received 5 QW doses (MAD1-MAD4) or 3 Q2W doses (MAD5, same dose amount as MAD4). The observed number of ADA positive (ADA pos) subjects for that dose panel is indicated with an asterisk. Histograms from the original model are orange (without Tregs), overlaid with histograms from the Treg adjusted model in blue (with Tregs)

the prediction of the SAD panels (Fig. 2, significant overlap between the orange and blue histograms). However, the presence of Tregs had a profound impact on the MAD panel predictions in all but the lowest MAD panel, with the blue histograms shifted to lower predicted ADA incidence more closely predicting the observed ADA incidence (Fig. 3). There was a relative decrease in predicted incidence rate of 21.5–59.3% across the MAD panels without compromising the single dose predictions (relative decrease in predicted incidence rate of 0.6–13%) (Table IV). The model predicted time course and magnitude of ADA response in the SAD using the Treg-adjusted model are shown in Fig. 4. The observed ADA data in units of nM were available to compare to the model predicted ADA for the SAD panels. The model was able to describe both the approximate time of onset (day 40 to day 70) and ADA concentrations observed in the trial with the exception of the lowest dose panel, where observed ADA concentrations were higher than predicted. One subject in the lowest dose SAD1 panel and one subject in the SAD5 panel were baseline ADA positive, and those patient data are not included in this analysis.

Model Predicted Impact on PK/PD

Since the model includes not only the generation of ADA, but also their ability to bind to (and potentially interfere with) the target binding, we further tested the model by investigating the PK and PD (as measured by free

Table IV. A Comparison of the Mean ADA+ Patients/Simulated Trial Between the Original and Treg Modified Models Along with the Observed ADA+ Patients. The Treg Model Is Predicting a Lower Mean That Is More Similar to the Observed Data Than the Original Model Without Tregs. The improved Model Predictability with Tregs Is More Notable in the Multidosing MAD Panels. The Mean Number of ADA+ Patients Was Computed Across 500 Simulated Trials from the Original Model and the Treg Supplemented Model

Panel	Observed ADA+ patients	Predicted mean (SD) ADA+ patients/trial Treg model	Predicted mean (SD) ADA+ patients/trial Original model	Relative change (%)
SAD1	3	0.2 (0.42)	0.2 (0.42)	−7.6
SAD2	2	1.4 (1.04)	1.4 (1.05)	−0.6
SAD3	4	3.4 (1.21)	3.7 (1.16)	−7.9
SAD4	2	4.2 (1.12)	4.6 (1.1)	−8.9
SAD5	3	4.5 (1.1)	5.1 (0.86)	−13.0
MAD1	3	3.6 (1.17)	4.6 (1.03)	−21.5
MAD2	4	6.4 (1.7)	10.6 (1.09)	−39.2
MAD3	4	5.6 (1.7)	10.9 (0.93)	−48.3
MAD4	3	4.7 (1.73)	11.5 (0.7)	−59.3
MAD5	3	5.6 (1.66)	11.1 (0.91)	−49.6

[a] %Relative change = $(ADA_{Treg}\text{-}ADA_{original})/ADA_{orginal} \times 100$

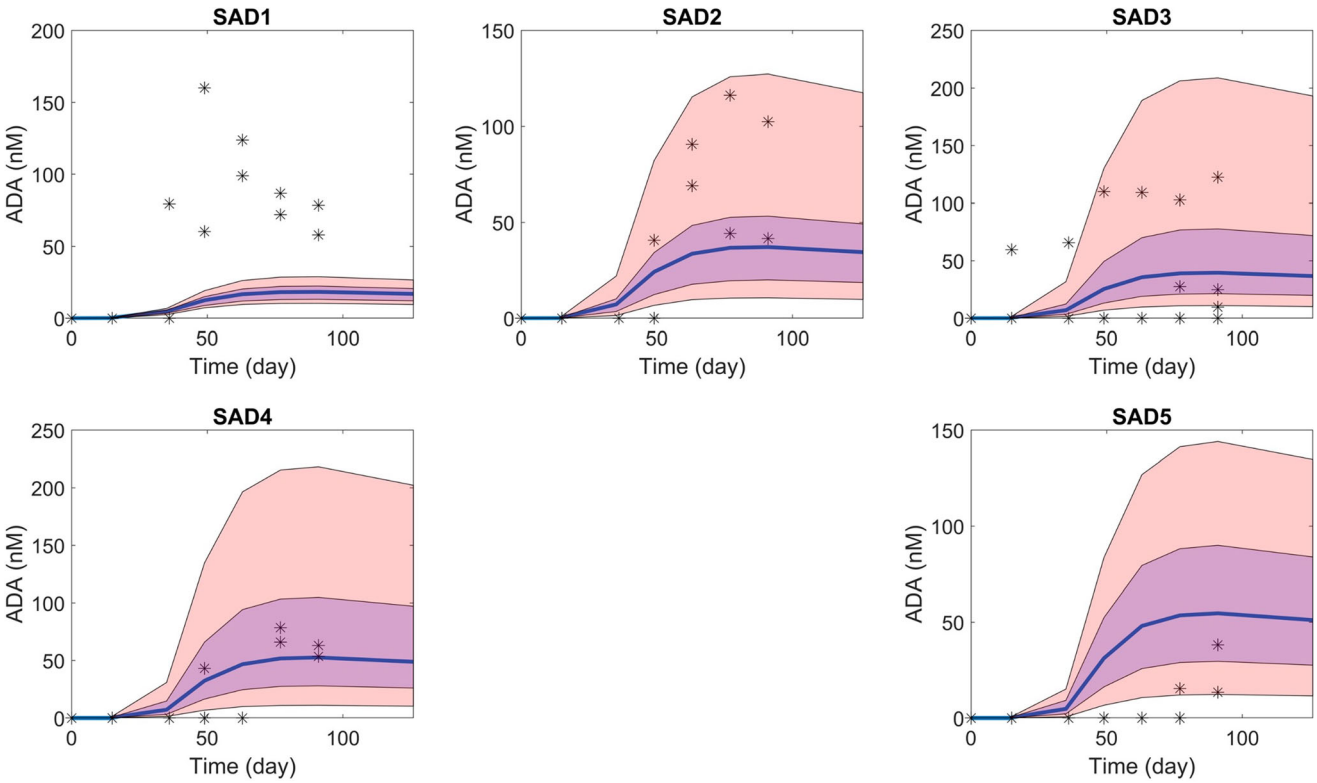

Fig. 4. The time course for predicted and observed ADA across all 5 SAD doses for the ADA positive subjects. The median prediction line is indicated along with the 95% prediction interval in pink and the interquartile range (IQR) in blue. Observed ADA is indicated as stars

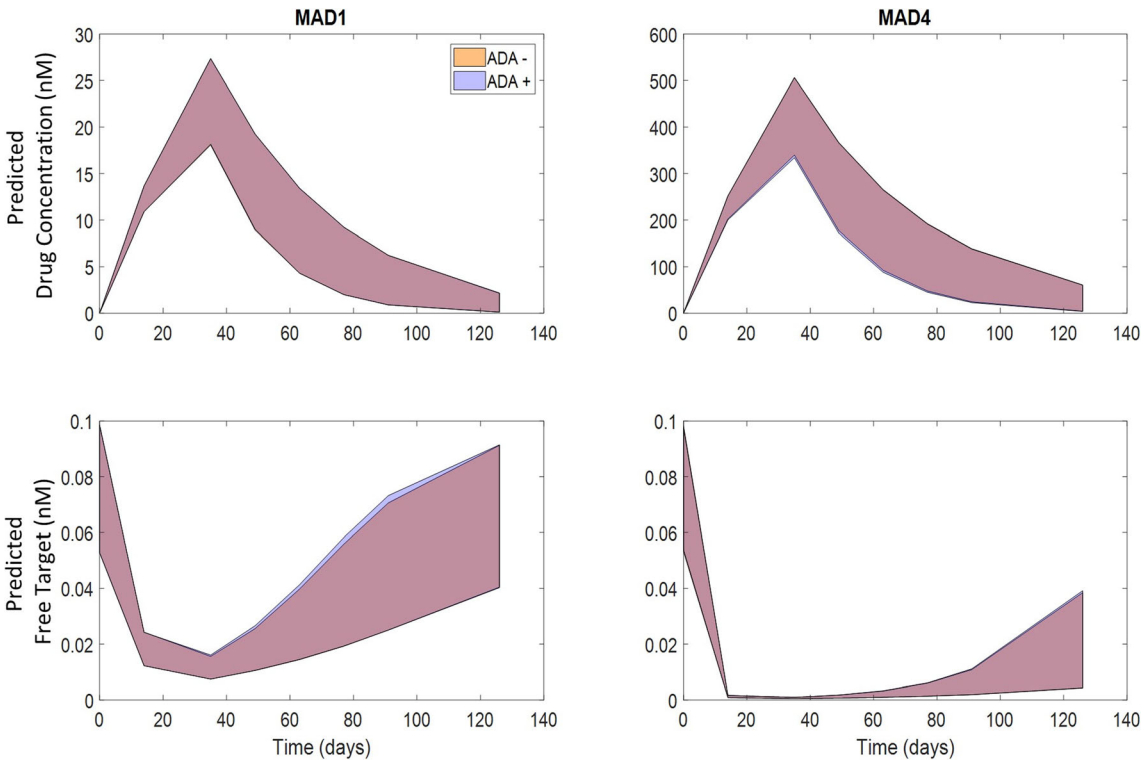

Fig. 5. PK (top panels) and PD (bottom panels) predicted over time for the MAD lowest and highest dose panels for ADA positive and ADA negative subjects. Similar trajectories for PK and PD were observed with 95% prediction intervals that completely overlap as indicated by the brown shaded regions

target lowering) in the MAD panels (Fig. 5). The median (95% CI) time course trajectories for ATI-1465 and free target are plotted for ADA positive subjects and ADA negative subjects (Fig. 5). The 95% CI intervals for positive and negative subjects completely overlapped and are indicated as one brown shaded region, indicating the model does not predict any discernible difference in the PK or immediate PD. This was consistent with the observed data for MAD1 where the ATI-1465 Cmax and AUC and the extent of target lowering were similar for ADA positive and negative subjects (Supplemental Table).

Model Predicted Impact of Oral Corticosteroid Concomitant Medication

As a final consideration of the possible utility of the model, we simulated the emergence of ADA over a 1 year virtual clinical trial duration using a weekly dosing schedule for three different dose levels (4, 20, and 50 mg) of ATI-1465. This biotherapeutic is intended to treat an indication where the patient population is typically on daily oral corticosteroids (OCS) as a standard of care with an expected OCS dose of approximately 20 mg prednisolone/day. Prednisolone has been shown to inhibit human whole blood lymphocyte proliferation (a sensitive parameter for ADA formation in the model, per the analysis in the CHV model (4,5)). Simulations of expected ADA incidence in the absence and presence of OCS leading to a 25% and 50% suppression of lymphocyte proliferation, and their impact on PD (% free target lowering during treatment) are shown in (Fig. 6). In the absence of OCS, the ADA incidence increased from the 4 to 20 mg ATI-1465 dose and plateaued at the 50 mg dose. Modeling a 25% reduction in the T and B cell proliferation rate dropped the ADA incidence to 0, 5 and 10% for the 4, 20 and 50 mg dose, respectively after 1 year of weekly dosing. At a 50% reduction in lymphocyte proliferation, no ADA is predicted for any dose level (Fig. 6). However, it is important to note that the immunosuppressive mechanistic effects of OCS are not well defined in general and considerations for the strength of the antigenic stimuli, total daily OCS dose and duration of treatment are additional important factors contributing to an antibody response (22).

DISCUSSION

The multiscale mechanistic model of immunogenicity described by Chen *et al.* (4,5) (CHV model) provides a conceptual framework for understanding the adaptive immune system biology and ADA production. The model is a logical extension of the current methods that are used to predict and evaluate ADA impact. In silico methods are used initially to predict peptide sequences that are potential T cell epitopes based on MHC-II binding affinities (7,22,23). Once antigenic sequences have been identified, in vitro experiments can be used to confirm peptide binding to MHCII (24), T cell proliferation and cytokine release (25,26). A mechanistic

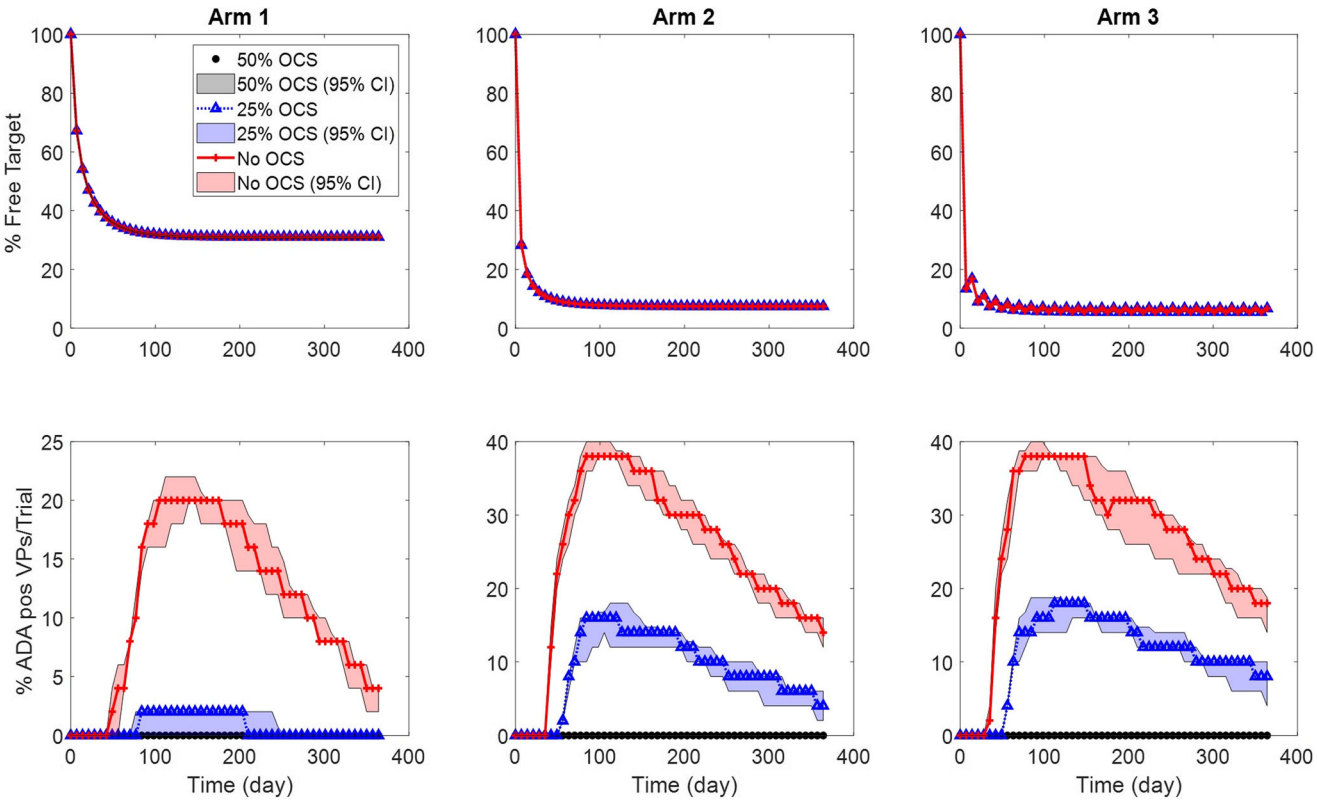

Fig. 6. The model can predict the impact of corticosteroid immunosuppression. Simulation of three different weekly doses over a 1-year duration using the Treg adjusted model. Three different oral corticosteroid (OSC) driven immunosuppression effects were simulated (0, 25, and 50% immunosuppression), and we show the median (line) and 90% CI of the resulting simulated trials. The number of ADA positive subjects (bottom panels) is reduced with increasing corticosteroid and the ADA impact on % target engagement (top panels) over time is not predicted to change

model can help bridge the in silico and in vitro predictions to downstream T and B cell biology that lead to antibody production and with a drug disposition model included, the longitudinal impact of ADA on biotherapeutic PK and PD can be evaluated.

Here we described the use the model to predict ADA for different doses, regimens, trial duration and corticosteroid use for ATI-1465, a biotherapeutic in phase 1 clinical development. The original CHV model could reasonably predict ADA for ATI-1465 after single dose, but there was a notable overprediction bias after multiple doses.

Treg Cell Adjusted Model

The original model had tolerance indirectly incorporated via decreased B cell proliferation rates at high antigen concentrations, but given the low levels of model predicted ADA for ATI-1465, thresholds for B cell tolerance were not met. Tolerance to an antigen could be invoked by a number of mechanisms that include both central tolerance (negative selection in the thymus) or peripheral tolerance that include sequestration of antigen, deletion or exhaustion (anergy) of autoreactive lymphocytes, upregulation of checkpoint receptors that dampen the response (*i.e.*, programmed death-1 (PD1)) or increases in Treg cells (27,28). Treg-induced tolerance was chosen to implement in this round of model optimization, given that Treg quantitative models were already published in the literature. Tolerance to an injected antigen, particularly after frequent exposure, is a well-documented phenomenon (29–34). Tolerance mechanisms are a form of protection to minimize inflammation-induced destruction of organ/tissues after frequent antigen exposures. Several hypotheses have been proposed for the mechanisms underlying tolerance, particularly in autoimmune disease where tolerance to self-Ag is dysfunctional (31). A quantitative, Teff and Treg cross regulation model of tolerance induction was previously described in the literature and used to update the CHV model (12). The premise behind the cross regulation model is that Treg cells have a negative effect on activated Teff cells, and Teff cells have a positive effect on the proliferation of Treg cells in a cross-regulated "prey-predator" system with Treg cells as the predator and Teff cells as the prey as described by Velez de Mendizabal *et al.* (12). The cross-regulation model was proposed for multiple sclerosis and although the model conceptually applies to healthy subjects, the number of Treg cells and their effects in autoimmune disease could potentially underestimate the tolerance effect in healthy subjects. After inclusion of the tolerance submodel, there was a notable decrease in the model predicted ADA incidence after multiple dosing, but not after single dose. This is consistent with the known physiology of tolerance where subsequent, multiple injections can stimulate higher populations of Treg cells (35).

The most noticeable differences between model-predicted and observed ADA occurred at the lowest dose panel after single dose (SAD 1, Fig. 2) and at the highest dose panel (SAD 5, Fig. 2). In each of these panels, there was one subject that had pre-existing ADAs, whose titers were boosted post-treatment. Pre-existing antibodies in patients have been described for some biotherapeutics, which can lead to treatment-boosted ADA increases (36,37). The current model does not account for this phenomenon and may explain why the model is under-predicting the ADA response for these two subjects.

Applications of a Multiscale Model of Immunogenicity

A mechanistic modeling approach that captures the biology of antigen recognition and downstream antibody production and its impact on PKPD has important applications. We were able to model the immunosuppressive effects of oral corticosteroids (OCS) with a model predicted reduction in ADA incidence with daily OCS administration. The immunosuppressive effect of corticosteroids on ADA formation could not have been predicted with more traditional empirical modeling methods that treat ADA as a covariate on drug clearance in the population PK model (38–41) or semi-mechanistic models of immunogenicity-mediated drug disposition (42) that lack the upstream mechanistic details on T and B cell proliferation that are needed to predict the corticosteroid effects. When ADA does impact PK or PD and there are no significant correlations of ADA with injection site reactions, hypersensitivities or other immune-mediated safety events, it may be possible to use the mechanistic model to design a dosing regimen that could maintain drug exposures above an efficacious threshold. In addition, when evaluating therapies that specifically up regulate (immuno-oncology therapies) or down regulate (anti-inflammatory therapies) the immune system, the impact of these mechanisms on ADA formation could be incorporated into the model.

Model Limitations and Future Development

While the current model has shown utility in predicting ADA for ATI-1465, there are several model assumptions and limitations that are important to emphasize to encourage additional model improvements. First, the antigen (biotherapeutic) system is equally distributed near the site of action, and the cellular and ADA responses are driven by the antigen concentration in the central compartment. The current model does not account for interactions that might take place in lymphoid compartments, where concentrations may not be reflective of plasma levels. Second, the virtual patients are completely antigen naïve at the start of the simulation and therefore any subjects that have pre-existing antibodies prior to treatment as was observed in our example cannot be accounted for in the model. Third, the model represents an otherwise healthy individual and a classical adaptive immune response with no competition for DC-mediated T cell activation or T cell-mediated B cell activation due to other disease processes. In addition modulatory cytokines are not currently included in the model. Fourth, the model assumes the in vitro predicted antigenic IC50 from the in silico screen translates in vivo. This could be an inaccurate assumption for some antigenic sequences and represent an overprediction of antigenicity since a relevant T cell repertoire is need for a response (43). Incorporating additional algorithms that offer improved predictions or confirming predicted antigenic sequences directly using MHC in vitro binding assays or human PBMCs could improve antigenicity predictions (43). Collecting HLA genotypes and evaluating pre and post treatment T cell repertoire expansion

could also help in the future to improve model predictions. Future development of this model will hopefully continue to evolve and gain acceptance as an additional tool to help describe and predict human immunogenicity.

CONCLUSION

This study demonstrates feasibility for using a mechanistic model of the immune system that captures fundamental biology of T and B cells responses to predict anti-ATI-1465 antibody in an early trial. The model was used to predict how anti-drug antibodies impact PKPD under different dosing regimens and immunosuppressive co-medications. Having a model based framework to predict and simulate how immunogenicity might change with different doses, schedules, immune-modulating co-meds, and HLA genetic background of the patients in a clinical trial will ultimately allow prospective planning and understanding of ADA impact on PK and efficacy.

ACKNOWLEDGMENTS

The authors wish to thank the patients from the early clinical trial for contributing valuable data to support the analysis. We would like to thank Xiaoying Chen, Tim Hickling, and Paolo Vicini who developed and published the Pfizer model for immunogenicity prediction and made their model code publically available, which enabled our work. The work was partially presented previously in poster form at the 6th American Conference on Pharmacometrics (ACoP) held in Crystal City, VA, USA, in October 2015, and published in the meeting proceedings as abstract T-018 (Article in Journal of Pharmacokinetics and Pharmacodynamics 42:S51-S51, October 2015).

AUTHOR CONTRIBUTIONS

All authors contributed to the design of the research. CT and LH wrote the manuscript. SC, AN, CT, and LH performed the research and analyzed data. CT conducted the modeling and simulation.

COMPLIANCE WITH ETHICAL STANDARDS

Conflict of Interest All authors were employees of Bristol-Myers Squibb at the time of this work.

REFERENCES

1. Deehan M, Garces S, Kramer D, Baker MP, Rat D, Roettger Y, et al. Managing unwanted immunogenicity of biologicals. Autoimmun Rev. 2015;14(7):569–74.
2. Baker MP, Reynolds HM, Lumicisi B, Bryson CJ. Immunogenicity of protein therapeutics: the key causes, consequences and challenges. Self Nonself. 2010;1(4):314–22.
3. Moticka EJ. Hallmarks of the adaptive immune response. In: Moticka EJ, editor. A historical perspective on evidence-based immunology. Waltham, MA: Elsevier; 2016. p. 9–19.
4. Chen X, Hickling TP, Vicini P. A mechanistic, multiscale mathematical model of immunogenicity for therapeutic proteins: part 2-model applications. CPT Pharmacometrics Syst Pharmacol. 2014;3:e134.
5. Chen X, Hickling TP, Vicini P. A mechanistic, multiscale mathematical model of immunogenicity for therapeutic proteins: part 1-theoretical model. CPT Pharmacometrics Syst Pharmacol. 2014;3:e133.
6. Cload *et al*. Fibronectin based scaffold domain proteins that bind to myostatin. United States Patent Application US20140107020A1, 2014.
7. Vita R, Overton JA, Greenbaum JA, Ponomarenko J, Clark JD, Cantrell JR, et al. The immune epitope database (IEDB) 3.0. Nucleic Acids Res. 2015;43(Database issue):D405–12.
8. Southwood S, Sidney J, Kondo A, del Guercio MF, Appella E, Hoffman S, et al. Several common HLA-DR types share largely overlapping peptide binding repertoires. J Immunol. 1998;160(7):3363–73.
9. U.S. National Library of Medicine NCfBI. BLASTP Suite for Protein Sequence Queries 2019 [Available from: https://blast.ncbi.nlm.nih.gov/Blast.cgi?PAGE=Proteins.
10. Tirucherai GS JL, Hamuro L, Ahlijanian M, Bechtold C and AbuTarif M. A target-mediated drug disposition model to characterize the PK-PD of BMS-986089 in healthy adults and its application to pediatric dose selection. ASCPT Abstracts. 2017.
11. Carneiro J, Leon K, Caramalho I, van den Dool C, Gardner R, Oliveira V, et al. When three is not a crowd: a crossregulation model of the dynamics and repertoire selection of regulatory CD4+ T cells. Immunol Rev. 2007;216:48–68.
12. Velez de Mendizabal N, Carneiro J, Sole RV, Goni J, Bragard J, Martinez-Forero I, et al. Modeling the effector - regulatory T cell cross-regulation reveals the intrinsic character of relapses in multiple sclerosis. BMC Syst Biol. 2011;5:114.
13. Maddur MS, Trinath J, Rabin M, Bolgert F, Guy M, Vallat JM, et al. Intravenous immunoglobulin-mediated expansion of regulatory T cells in autoimmune patients is associated with increased prostaglandin E2 levels in the circulation. Cell Mol Immunol. 2015;12(5):650–2.
14. Mukhopadhyay S, Varma S, Mohan Kumar HN, Yusaf J, Goyal M, Mehta V, et al. Circulating level of regulatory T cells in rheumatic heart disease: an observational study. Indian Heart J. 2016;68(3):342–8.
15. Wilson LD, Zaldivar FP, Schwindt CD, Wang-Rodriguez J, Cooper DM. Circulating T-regulatory cells, exercise and the elite adolescent swimmer. Pediatr Exerc Sci. 2009;21(3):305–17.
16. Mager DE, Moledina N, Jusko WJ. Relative immunosuppressive potency of therapeutic corticosteroids measured by whole blood lymphocyte proliferation. J Pharm Sci. 2003;92(7):1521–5.
17. Rohatagi S, Barth J, Mollmann H, Hochhaus G, Soldner A, Mollmann C, et al. Pharmacokinetics of methylprednisolone and prednisolone after single and multiple oral administration. J Clin Pharmacol. 1997;37(10):916–25.
18. Xu J, Winkler J. Derendorf H. a pharmacokinetic/pharmacodynamic approach to predict total prednisolone concentrations in human plasma. J Pharmacokinet Pharmacodyn. 2007;34(3):355–72.
19. Karosiene E, Rasmussen M, Blicher T, Lund O, Buus S, Nielsen M. NetMHCIIpan-3.0, a common pan-specific MHC class II prediction method including all three human MHC class II isotypes, HLA-DR, HLA-DP and HLA-DQ. Immunogenetics. 2013;65(10):711–24.
20. The dbMHC database provides an open, publicly accessible platform for DNA and clinical data related to the human Major Histocompatibility Complex (MHC). Produced and maintained in cooperation with the Medical University Graz, Austria. [Available from: https://www.ncbi.nlm.nih.gov/gv/mhc/main.fcgi?cmd=init.
21. 2010–2102 CoID. Section 1: active and passive immunization: immunocompromised children. Red book: 2012 report of the Committee on Infectious Diseases. 29th ed. Elk Grove Village: American Academy of Pediatrics; 2012. p. 81–2.
22. Bryson CJ, Jones TD, Baker MP. Prediction of immunogenicity of therapeutic proteins: validity of computational tools. BioDrugs. 2010;24:1):1–8.

23. De Groot AS, Martin W. Reducing risk, improving outcomes: bioengineering less immunogenic protein therapeutics. Clin Immunol. 2009;131(2):189–201.
24. Caron E, Kowalewski DJ, Chiek Koh C, Sturm T, Schuster H, Aebersold R. Analysis of major histocompatibility complex (MHC) immunopeptidomes using mass spectrometry. Mol Cell Proteomics. 2015;14(12):3105–17.
25. Faulkner L, Gibson A, Sullivan A, Tailor A, Usui T, Alfirevic A, et al. Detection of primary T cell responses to drugs and chemicals in HLA-typed volunteers: implications for the prediction of drug immunogenicity. Toxicol Sci. 2016;154(2):416–29.
26. Karle A, Spindeldreher S, Kolbinger F. Secukinumab, a novel anti-IL-17A antibody, shows low immunogenicity potential in human in vitro assays comparable to other marketed biotherapeutics with low clinical immunogenicity. MAbs. 2016;8(3):536–50.
27. Schwartz RH. Historical overview of immunological tolerance. Cold Spring Harb Perspect Biol. 2012;4(4):a006908.
28. Szczepanik M. Mechanisms of immunological tolerance to the antigens of the central nervous system. Skin-induced tolerance as a new therapeutic concept. J Physiol Pharmacol. 2011;62(2):159–65.
29. Boer MC, Joosten SA, Ottenhoff TH. Regulatory T-cells at the interface between human host and pathogens in infectious diseases and vaccination. Front Immunol. 2015;6:217.
30. Joosten SA, Ottenhoff TH. Human CD4 and CD8 regulatory T cells in infectious diseases and vaccination. Hum Immunol. 2008;69(11):760–70.
31. Miller SD, Turley DM, Podojil JR. Antigen-specific tolerance strategies for the prevention and treatment of autoimmune disease. Nat Rev Immunol. 2007;7(9):665–77.
32. Sakaguchi S, Yamaguchi T, Nomura T, Ono M. Regulatory T cells and immune tolerance. Cell. 2008;133(5):775–87.
33. Takahashi T, Kuniyasu Y, Toda M, Sakaguchi N, Itoh M, Iwata M, et al. Immunologic self-tolerance maintained by CD25+CD4+ naturally anergic and suppressive T cells: induction of autoimmune disease by breaking their anergic/suppressive state. Int Immunol. 1998;10(12):1969–80.
34. von Herrath MG, Harrison LC. Antigen-induced regulatory T cells in autoimmunity. Nat Rev Immunol. 2003;3(3):223–32.
35. Anderson PO, Manzo BA, Sundstedt A, Minaee S, Symonds A, Khalid S, et al. Persistent antigenic stimulation alters the transcription program in T cells, resulting in antigen-specific tolerance. Eur J Immunol. 2006;36(6):1374–85.
36. Xue L, Fiscella M, Rajadhyaksha M, Goyal J, Holland C, Gorovits B, et al. Pre-existing biotherapeutic-reactive antibodies: survey results within the American Association of Pharmaceutical Scientists. AAPS J. 2013;15(3):852–5.
37. Xue L, Rup B. Evaluation of pre-existing antibody presence as a risk factor for posttreatment anti-drug antibody induction: analysis of human clinical study data for multiple biotherapeutics. AAPS J. 2013;15(3):893–6.
38. Gomez-Mantilla JD, Troconiz IF, Parra-Guillen Z, Garrido MJ. Review on modeling anti-antibody responses to monoclonal antibodies. J Pharmacokinet Pharmacodyn. 2014;41(5):523–36.
39. Perez Ruixo JJ, Ma P, Chow AT. The utility of modeling and simulation approaches to evaluate immunogenicity effect on the therapeutic protein pharmacokinetics. AAPS J. 2013;15(1):172–82.
40. Thway TM, Magana I, Bautista A, Jawa V, Gu W, Ma M. Impact of anti-drug antibodies in preclinical pharmacokinetic assessment. AAPS J. 2013;15(3):856–63.
41. Wang YM, Jawa V, Ma M. Immunogenicity and PK/PD evaluation in biotherapeutic drug development: scientific considerations for bioanalytical methods and data analysis. Bioanalysis. 2014;6(1):79–87.
42. Parra-Guillen ZP, Janda A, Alzuguren P, Berraondo P, Hernandez-Alcoceba R, Troconiz IF. Target-mediated disposition model describing the dynamics of IL12 and IFNgamma after administration of a mifepristone-inducible adenoviral vector for IL-12 expression in mice. AAPS J. 2013;15(1):183–94.
43. Gokemeijer J, Jawa V, Mitra-Kaushik S. How close are we to profiling immunogenicity risk using in silico algorithms and in vitro methods?: an industry perspective. AAPS J. 2017;19(6):1587–92.